Cu(In,Ga)Se_2 absorbers from stacked nanoparticle precursor layers

A.R. Uhl[1]*, M. Koller[1], A.S. Wallerand[1], C.M. Fella[1], L. Kranz[1], H. Hagendorfer[1], Y.E. Romanyuk[1], A.N. Tiwari[1], S. Yoon[2], A. Weidenkaff[2], T.M. Friedlmeier[3], E. Ahlswede[3], D. VanGenechten[4], F. Stassin[4]

[1]Laboratory for Thin Films and Photovoltaics, Empa, Swiss Federal Laboratories for Materials Science and Technology, 8600 Duebendorf, Switzerland; [2]Laboratory for Solid State Chemistry and Catalysis, Empa, Swiss Federal Laboratories for Materials Science and Technology, 8600 Duebendorf, Switzerland; [3]Zentrum für Sonnenenergie- und Wasserstoff-Forschung (ZSW), 70565 Stuttgart, Germany; [4]Umicore S.A., 2250 Olen, Belgium

Abstract:

The following paper presents a processing route for Cu(In,Ga)Se_2 absorber layers that is based on nanoparticle dispersions which are applied by doctor blade deposition and converted with elemental selenium vapors. In particular, the preparation of the precursor layers is investigated by systematically assessing the influence of the stacking sequence of mono- and multi-metallic layers on sintering, elemental distribution and solar cell efficiency. By applying suitable stacking sequences, precursor layers with both local Cu-rich and over-all Cu-poor stoichiometry could be prepared that allowed improved sintering properties and modifications of the gallium gradient. Despite the still prevailing porosity of the absorber layer, solar cells with efficiencies exceeding 5% could be obtained.

*corresponding author: alexander.uhl@empa.ch, phone: +41-58-7656104

Introduction

Solar cells based on Cu(In,Ga)Se_2 (CIGS) absorber layers have shown the highest efficiency amongst all thin film technologies [1]. For record devices the absorber layer is typically deposited via co-evaporation method from the elements, allowing for the controlled deposition of high purity layers. Most research groups follow the "three stage process": first, a $(InGa)_xSe_y$ compound is deposited; this is followed by the deposition of Cu and Se until the film has an overall Cu-rich composition; and finally, In and Ga are added to bring the composition back to Cu-deficient [2,3]. The efficiency gain has been attributed to both electronic and structural reasons: the formation of a double Ga-gradient that exhibits enhanced solar light absorption due to a low minimum band gap, increased minority carrier collection at the back contact due to the introduction of a back surface field, and improved V_{OC} due to elevated built in voltage at the front contact. Structurally, it was shown that the Cu-rich growth phase results an improved grain size and morphology [2-6].

In contrast to that, a single graded absorber is typically obtained for selenization processes. The higher Ga/III content near the back contact is formed spontaneously due to different formation rates of CIS and CGS during a selenization process that is initiated from the top [6,7]. Overcoming this limitation, researchers have widened the absorber band gap at the surface by post sulfurization treatments, but highly reactive gases, i.e. H_2S, had to be utilized to ensure the anion substitution [8,9]. Selenization processes of sputtered or printed precursor layers have gained wide attention at an industrial scale due to favorable large scale uniformity. Printing processes in particular excel with low capital investment, high throughput, and high material utilization. Both solutions and particle dispersions have been employed and have shown remarkable efficiencies up to 15.2% [10] and 17.1% [11,12]. However, toxic and explosive solvents or gases often have to be employed for complete dissolution or conversion/reduction of metal oxides particles.

In this paper, we present a novel process based on the conversion of hydroxide particles by selenium vapors. The chemical coordination of the particle and a deposition method of multiple “stacked” precursor layers with varying chemical composition allowed improved sintering and fabrication of a double Ga-gradient while omitting the use of H_2 or H_2Se/H_2S gases.

Experimental Details:

Three individual nanoparticle inks based on Cu-, In-, and Ga-hydroxides were employed, allowing the stoichiometric adjustment of the final precursor layer by means of adequate mixing ratio or sequential processing. In the standard process, the composition was tailored to be Cu/III = 0.80 and Ga/III = 0.25, as confirmed by XRF measurements. The dispersions were deposited by knife coating technique on molybdenum coated glass slides heated to 80°C, with a substrate to knife distance of 50 µm, and a blading speed of 50 mm/s. The obtained precursor film was dried at 200°C for three minutes and subsequently selenized in a two-temperature zone selenization furnace as previously described [13].

For multilayer deposition the drying and deposition step was repeated three times with varying precursor ink at a reduced substrate to knife distance of 20, 20, and 10 µm. The selenization time at 550°C was 35 minutes. Selenized films were treated by KCN etching step to remove any residual Cu-Se binary phases and then coated by a ~50 nm thick buffer layer of CdS that was deposited by chemical bath deposition.

The solar cell was finalized by RF-sputtering of a i-ZnO/ZnO:Al window layer and mechanical scribing to 9 mm^2 cell area. The current voltage characteristic was then measured at simulated AM1.5 solar irradiation under standard test conditions.

Morphological and compositional analysis was conducted using X-ray fluorescence spectroscopy (XRF) from a rhodium target at 45 kV, powder x-ray diffraction (XRD) on a Siemens D5000 diffractometer with Ni-filtered Cu-Kα radiation, scanning electron microscopy (SEM) and energy dispersive X-ray spectroscopy (EDX) on a Hitachi S-4800, time-of-flight secondary ion mass spectroscopy (ToF-SIMS) by a ION-TOF TOF.SIMS 5 ION-TOF using Bi^+ as the primary ion for the analysis (25 kV, 1 pA, 100 x 100 μm^2) after a two second sputter cycle with O^{2+} for the depth profile analysis (2 kV, 400 nA, 300 x 300 μm^2). Inductively coupled plasma mass spectrometry measurements (ICPMS) were performed with an Agilent 7500cs ICPMS with Merck ICPMS single element standards (0.1 - 10000 µg/l). In-situ XRD was carried out using a PANalytical X'Pert Pro MPD system in grazing angle geometry at an incident angle of 10°. The substrate heating at 5 °C/min was done with an Anton-Paar XRK 900 heating chamber. Surrounding Se pellets, a Se top layer as well as a graphite dome covering the sample ensured sufficient Se supply during the measurement. The graphite dome, however, contributed to the obtained diffractograms with additional carbon reflections (PDF No. 26-1079).

Results and Discussion

Morphological comparison of stacks and mixtures

Hydroxide nanoparticle inks were used in this study to omit the need of H_2 reduction while being able to achieve complete conversion by means of elemental Se vapors. This concept was proven by EDX measurements of selenized films that resulted in stoichiometric amounts of selenium with no detectable amounts of residual oxygen and carbon (dried precursor: C = 15 at.%, O = 60 at.%, selenized film: C = 0 at.%, O = 0 at.%). Absorber layers from these mixed precursors, however, appeared porous with small grain size and micro cracks, as seen in Fig. 1a.

While a copper-rich growth phase is commonly used in vacuum deposition of CIGS to improve grain growth, less research has been carried out for nanoparticulate precursors. To mimic the idea of a copper-

rich growth phase while keeping an overall Cu-poor stoichiometry to avoid shunting Cu-Se segregations, a multilayer approach was studied. In the latter, a locally Cu-rich layer in form of a Cu-precursor film was surrounded by a top and bottom layer of mixed Ga and In precursor. In comparison to results from mixed particle precursors, it is apparent in Fig. 1b that the morphology significantly changed. Cross-section SEM images reveal a porous intermediate layer at the position of former Cu-precursor. While top-view SEM pictures indicate improved sintering of the top layer, large grained segregations of $CuInSe_2$ and $Cu_{2-x}Se$ – as confirmed by EDX – appear on the surface. It should be noted that the overall stoichiometry as obtained from ICPMS measurements from selenized precursors was Cu/III = 0.80, Ga/III = 0.25 for the mixture and Cu/III = 0.74, Ga/III = 0.25 for the stack, showing that improved sintering was feasible even though a lower Cu-content was present.

Reaction kinetics with in-situ XRD

To further elucidate the origin of morphological changes, in-situ XRD measurements have been conducted for both mixed and stacked precursors. Figure 2 shows the temperature evolution of the respective diffractograms. Neglecting the carbon reflections from the graphite peak around 26.3° and 42.6°, the low temperature regime from 100 to 220°C is dominated by the crystallization of the Se top layer (PDF No. 42-1425). Above that temperature selenium is molten and available for metal conversion. In the mixed precursor approach the formation of $Cu_{2-x}Se$ (PDF Nr. 46-1129) is visible at around 270°C while Cu is more readily converted for stacked precursors. Here, the $CuSe_2$ formation is visible as cubic (PDF Nr. 01-071-0047) and orthorhombic form (PDF Nr. 19-0400) from 220 - 280°C and 240 - 310°C, respectively. At 310°C, $CuSe_2$ seems to be converted into CuSe (PDF Nr. 49-1457) which is prevailing until 350°C. Also the selenium poor $Cu_{2-x}Se$ phase is visible between 240°C to 350°C. In the case of mixed particles, it is the $Cu_{2-x}Se$ phase alone that appears and remains until 440°C. For both cases first CIS reflections (PDF Nr. 40-1487) appear around 300°C and are accompanied by $MoSe_2$ (PDF Nr. 01-077-1715) at around 440°C. The resulting films appear phase pure for both cases with last secondary phases disappearing at 440°C and 350°C for mixtures and stacks, respectively. Thus, it can be suggested that the local separation of Cu in the stacked approach leads to pronounced formation of binary selenides with high reactivity, as seen by their formation and consumption at lower temperatures.

The high diffusivity of the Cu-Se phases could explain, in part, the improved sintering behavior in the case of the stacked precursor layers [14-17]. However, as Cu-Se appears more mobile than other phases, it is responsible for the void after selenization at the position of the Cu-layer as well as segregations to the top (see Fig. 1).

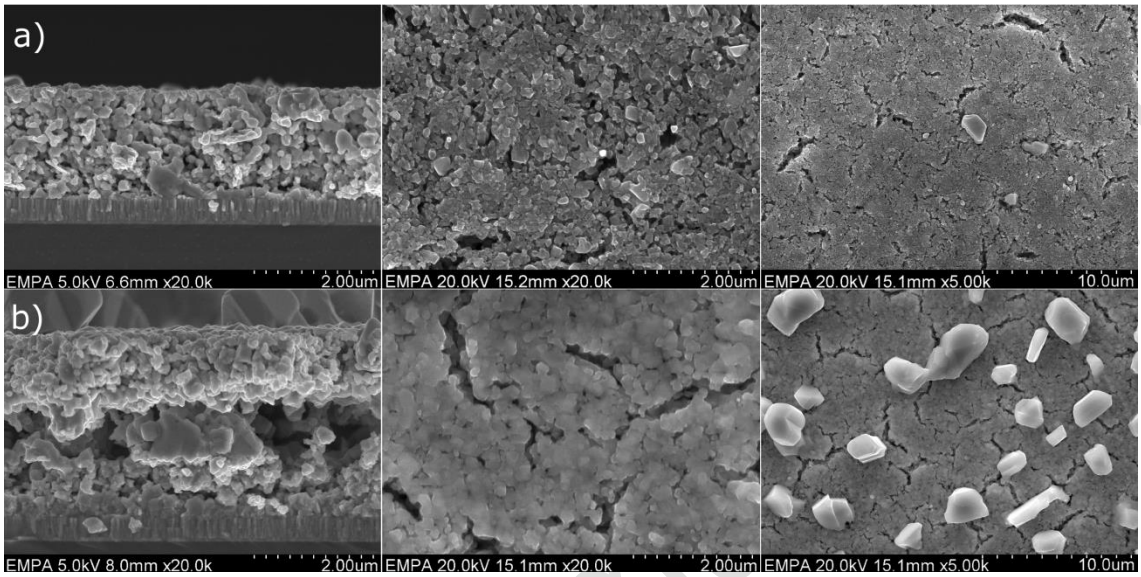

Fig. 1. Top-view and cross-section scanning electron micrographs of selenized precursor layers on Mo coated soda-lime glass substrates. Absorber from mixed metal precursors (a) results in porous morphology with small crystallites whereas absorbers from stacked precursor layers (b) exhibit the formation of a porous intermediate layer at the position of Cu-precursor. As the crystallites in the latter case increase, large grained segregations of $CuInSe_2$ and $Cu_{2-x}Se$ – as confirmed by EDX – appear on the surface.

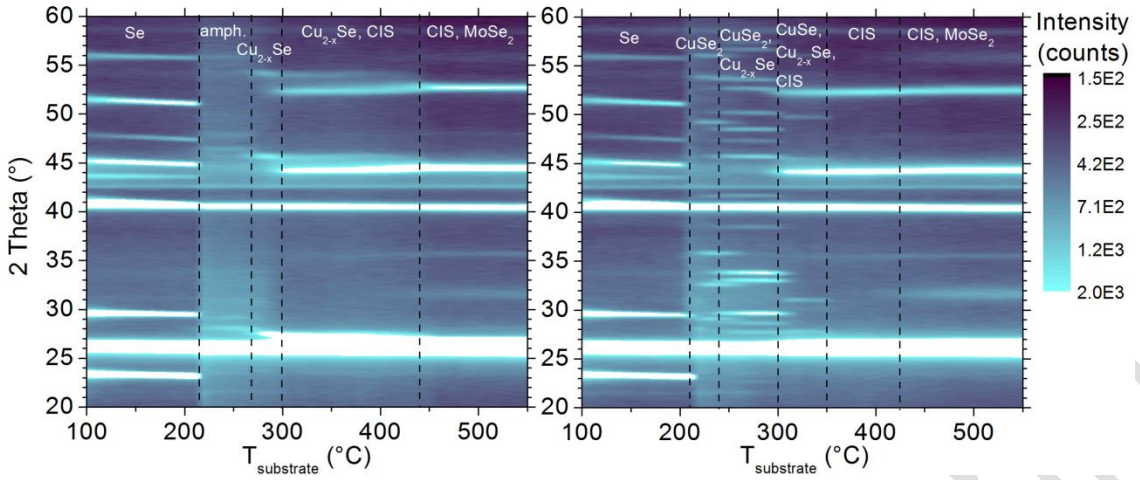

Fig. 2. In-situ XRD measurements during selenization of mixed (left) and stacked precursor setup (right). The color table shows the obtained intensity in counts. These model experiments visualize the formation of binary selenides during the reaction to CI(G)S. While only $Cu_{2-x}Se$ is formed between 270 - 440°C in the mixed precursor case, the stacked approach shows varying Cu-Se phases between 220 - 350°C including cubic $CuSe_2$, orthorhombic $CuSe_2$, CuSe, and $Cu_{2-x}Se$.

Compositional analysis

Powder XRD measurements were carried out for selenized layers from mixed and stacked precursors to investigate the phase purity of the absorber. Figure 3 shows the diffraction patterns of the CIGS (220/204) reflection for both precursor types. Due to the overlap of binary $Cu_{2-x}Se$ with $Cu(In_{0.7}Ga_{0.3})Se_2$, measurements were conducted both before and after a KCN etching treatment. As expected from EDX results no reflections from Ga_2O_3 (PDF Nr. 06-0503) or In_2O_3 (PDF Nr. 44-1087) were visible in the diffractograms, confirming complete the precursor conversion into the selenide phase. Comparing the dashed and solid lines it is apparent that some amount of Cu-Se binary phases is removed by KCN etching for both precursor types. For KCN etched samples, the peak shift to higher angles can be attributed to higher levels of gallium incorporation into the CIS crystal structure. As the gallium incorporation is quite uniform and shows only a single reflection around Ga/III = 0.30 for the mixed precursor, a vast compositional gradient is observed for the precursor stacks. The composition varies from pure CIS to Ga/III = 0.35 for the latter case.

In order to see the lateral distribution of these compositional gradients, SIMS measurements were conducted. Figure 4 depicts the Ga/III depth profiles of absorber layers from mixed and stacked precursor layers. SIMS measurements were calibrated to fit the ICPMS determined average composition of Ga/III = 0.25, respectively. As is commonly observed for selenization processes a weak single gradient is visible for absorber from mixed precursors exhibiting higher gallium content towards the back contact. This phenomenon could be a result of the provision of selenium from the surface and the lower reactivity of Ga as compared to Cu and In. A different and more pronounced gradient, however, is observed for absorbers from stacked precursor layers. Here, the surface composition is Ga-poor, i.e. Ga/III = 0.22 - 0.24, increases towards Ga/III = 0.27 in the first quarter of the absorber, drops again to Ga/III = 0.24 in the absorber middle to increase again to Ga/III = 0.27 towards the back contact. Disregarding the large grained segregations of $Cu_{2-x}Se$ and CIS on the surface of the absorber that lower the Ga/III ratio on the absorber front, the profile can be described as a gallium double-gradient. This is remarkable for a selenization process and can again be explained with reference to the surface provision of selenium and a competing kinetic reaction of CIS and CGS. Similarly to the three-stage-process during vacuum evaporation, the intermediate Cu-layer that is surrounded by a mixed In + Ga layer will preferably react with indium rather than gallium to form a spontaneous Ga-double gradient. The high mobility of Cu-Se and the selenium provision from the surface could explain the $Cu_{2-x}Se$ and CIS segregations on the absorber surface.

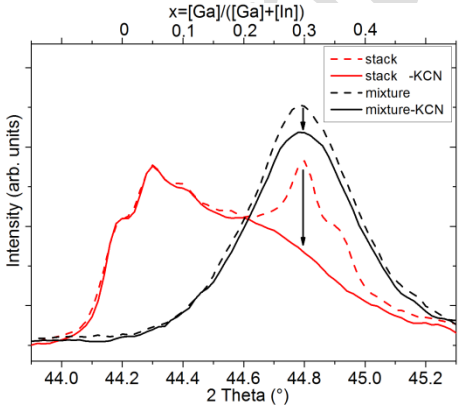

Fig. 3. X-ray diffraction patterns of the CIGS (220/204) reflection for mixed and stacked precursors after selenization. The arrows indicate the removal of Cu-Se binary phase after selective KCN etching.

Absorbers from stacked precursors exhibit a wide compositional gradient in terms of Ga incorporation while absorbers from mixtures show more uniform Ga distribution.

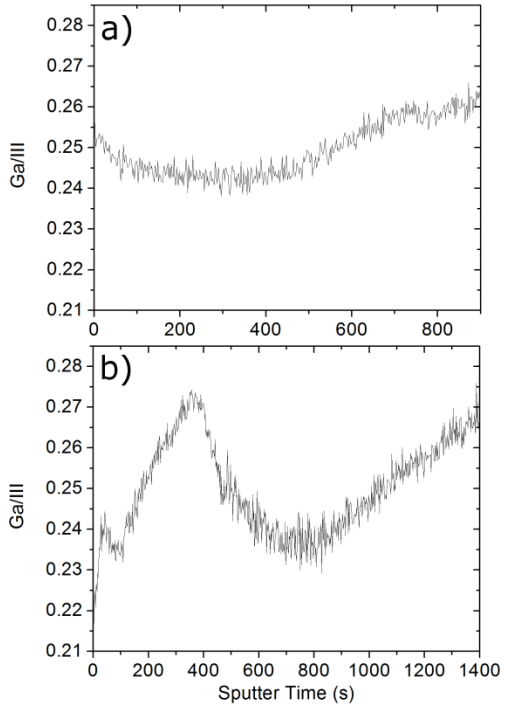

Fig. 4. Compositional Ga/III profile of absorber layers from SIMS measurements calibrated with ICPMS. A single and double Ga-gradient is visible for mixture (a) and stacked layer (b), respectively. Please note that low Ga/III at the surface of stacks stems from Cu-Se/CIS segregations that are visible in SEM/EDX.

Device performance

Absorbers from both mixed and stacked precursor layers were processed into solar cells of 9 mm^2 area without antireflection coating and their electrical performance has been measured. Fig. 5 shows the external quantum efficicency (EQE(λ)) and the current density-voltage characteristics (J(V)) of two champion devices. Comparing the EQE(λ) data of both processes it is apparent that absorbers from stacked precursor layers exhibit a higher spectral response in the long wavelength region resulting in a gain in short circuit current density J_{SC}. As shown in the inset graph, a minimum band gap of 1.0 eV and 1.2 eV can be calculated from the absorption onsets which is in good agreement with previously shown XRD measurements. Despite the still prevailing porosity, efficiencies of up to 4.8% and 5.8% could be

achieved for non-vacuum absorbers from mixed and stacked precursor layers, respectively. The gain in efficiency for the stacked approach can be explained mainly due to improved series and shunt resistances next to increased J_{SC} as described earlier. The porosity of the absorber layer introduces both high R_S through small connections of absorber grains as well as a small R_P due to the high likelihood of shunt paths introduced through covering layers. The denser and larger grained top layer in the stacked precursor approach might have contributed to the efficiency improvement.

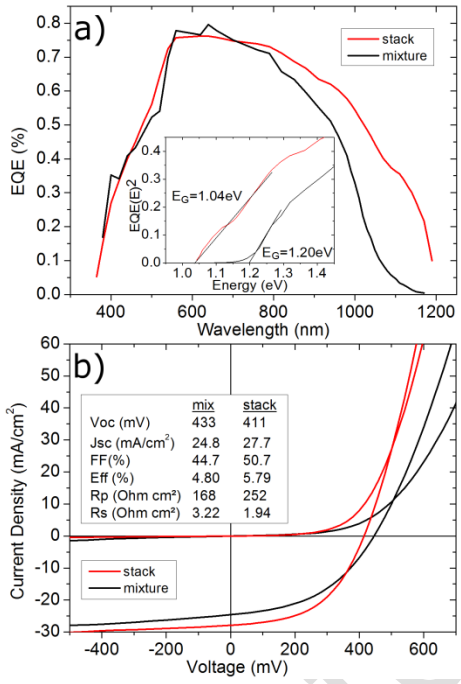

Fig. 5. External quantum efficiency (a) and current density- voltage measurements (b) for two champion devices from absorbers from mixed and stacked precursors showing up to 4.8% and 5.8% efficiency, respectively (total area, 9 mm^2, without AR-coating). While absorbers from the stacked approach exhibit a lower minimum band gap and thus higher J_{SC}, the main efficiency gain is attributed to improved series and parallel resistances.

Conclusion

$Cu(In,Ga)Se_2$ absorber layers were fabricated by a process based on the non-vacuum deposition of hydroxide containing particles and the conversion by selenium vapors without the need of a chemical

reduction step. EDX and SEM cross-sections confirmed that absorbers appear free from oxygen and carbon residuals, i.e. carbon-rich layers that were previously observed for solution approaches [18,19]. Precursor layers were fabricated from mixed and stacked precursor layers with consecutive depositions of In+Ga/ Cu/ In+Ga. It was found that while absorbers from the former approach appeared mainly porous, absorbers from the latter showed improved sintering properties especially at the positions of group IIIA layers. The appearance of a void layer at the position of previous Cu-precursor and surface segregations of $Cu_{2-x}Se$ and CIS to the top suggest a high mobility of Cu species. In-situ XRD measurements showed the formation of $CuSe_2$, CuSe and $Cu_{2-x}Se$ from 220 - 350°C for the stacked approach while only $Cu_{2-x}Se$ was visible from 270 - 440°C for the mixed precursor case. It could be shown that the spontaneous band gap grading for selenization processes, i.e. higher Ga/III towards the back contact, could be altered in the case of the stacking approach. By means of XRD and SIMS measurements, the formation of a double Ga-gradient below the Ga-free segregations on the surface can be suggested. The absorption onset at high wavelengths during EQE(λ) measurements confirms the formation of Ga-free absorber material for the stacked approach. J(V) comparisons between mixtures and stacks show improvements mainly in R_S and R_P that could be in accordance to improved sintering of the top layer. Despite the prevailing porosity of obtained absorber layers, surface segregation, and large compositional gradients, conversion efficiencies up to 5.8% could be obtained, highlighting the concept of stacked hydroxide based nanoparticulate precursor layers for the formation of CIGS absorbers. By smoothening the stacking sequences further improvements are expected from improved sintering, reduced surface segregation and less tailored Ga-gradients.

Acknowledgements

This work was conducted in the framework of the European FP7 project “NOVA-CIGS”.

References:

[1] P. Jackson, D. Hariskos, E. Lotter, S. Paetel, R. Wuerz, R. Menner, W. Wischmann, M. Powalla, Prog. Photovolt. Res. Appl. 19 (2011) 894, doi:10.1002/pip.1078.

[2] A.M. Gabor, J.R. Tuttle, D.S. Albin, M.A. Contreras, R. Noufi, Appl. Phys. Lett. 65 (1994) 198, doi: 10.1063/1.112670.

[3] A.M. Gabor, J.R. Tuttle, M.H. Bode, A. Franz, A.L. Tennant, M.A. Contreras, R. Noufi, D.G. Jensen, A.M. Hermann, Sol. Energy Mater. Sol. Cells, 41–42 (1996) 247.

[4] J. Song, S.S. Li, C.H. Huang, O.D. Crisalle, T.J. Anderson, Solid State Electron. 48 (2004) 73.

[5] T. Dullweber, G. Hanna, U. Rau, H.W. Schock, Sol. Energy Mater. Sol. Cells 67 (2001) 145.

[6] O. Lundberg, Ph.D. Thesis, Faculty of Science and Technology, Uppsala University, Sweden, 2003.

[7] F. Hergert, R. Hock, A. Weber, M. Purwins, J. Palm, V. Probst, J. Phys. Chem. Solids 66 (2005) 1903.

[8] T. Nakada, H. Ohbo, T. Watanabe, H. Nakazawa, M. Matsui, A. Kunioka, Sol. Energy Mater. Sol. Cells 49 (1997) 285.

[9] D. Tarrant, J. Ermer, Conference Record of the 23rd IEEE Photovoltaic Specialists Conference, Louisville, KY, 1993, p. 372.

[10] T.K. Todorov, O. Gunawan, T. Gokmen, D.B. Mitzi, Prog. Photovolt. Res. Appl. (2012), doi: 10.1002/pip.1253

[11] C. Eberspacher, K.Pauls, J. Serra, Conference Record of the 29th IEEE Photovoltaic Specialists Conference, New Orleans, LA, 2002, p. 684.

[12] Nanosolar Inc., Nanosolar Communications, San Jose, CA, 2011 http://www.nanosolar.com/company/blog/nanosolar-achieves-171-aperture-efficiency-through-printed-cigs-process

[13] A.R. Uhl, Y.E. Romanyuk, A.N. Tiwari, Thin Solid Films 519 (2011) 7259, doi:10.1016/j.tsf.2011.01.136

[14] M. Casteleyn, M. Burgelman, B. Depuydt, A. Niemegeers, I. Clemminck, Conference Record of the 24th IEEE Photovoltaic Specialists Conference, Waikola, HI, 1994, p. 230

[15] A. Brummer, V. Honkimäki, P. Berwian, V. Probst, J. Palm, R. Hock, Thin Solid Films 437 (2003) 297.

[16] F. Hergert, S. Jost, R. Hock, M. Purwins, J. Solid State Chem. 179 (2006) 2394.

[17] W.K. Kim, S. Kim, E.A. Payzant, S.A. Speakman, S. Yoon, R.M. Kaczynski, R.D. Acher, T.J. Anderson, O.D. Crisalle, S.S. Li, V. Craciun, J. Phys. Chem. Solids 66 (2005) 1915.

[18] C.M. Fella, A.R. Uhl, Y.E. Romanyuk, A.N. Tiwari, Phys. Status Solidi A 209 (2012) 1043, doi: 10.1002/pssa.201228003.

[19] A.R. Uhl, C. Fella, A. Chirila, M.R. Kaelin, L. Karvonen, A. Weidenkaff, C.N. Borca, D. Grolimund, Y.E. Romanyuk, A.N. Tiwari, Prog. Photovolt. Res. Appl. 20 (2012) 526, doi:10.1002/pip.1246.